Progress In Electromagnetics Research M, Vol. 31, 279–293, 2013

A 3-D UNCONDITIONALLY STABLE LAGUERRE-RPIM MESHLESS METHOD FOR TIME-DOMAIN ELECTROMAGNETIC COMPUTATIONS

Feijiao Liu*, Donglin Su, and Yilong Zhang

School of Electronic and Information Engineering, Beihang University, Haidian, Beijing 100191, China

Abstract—In this paper, a 3-D unconditionally stable meshless method is introduced to simulate time-domain electromagnetic problems. It combines the conventional radial point interpolation method (RPIM) and weighted decaying Laguerre polynomials together to discrete Maxwell's differential equations. The new method called Laguerre-RPIM retains the advantages of both the node-based meshless method and the unconditionally stable scheme of weighted Laguerre polynomials. The accuracy and efficiency of the proposed method are verified through two numeral examples. It can be seen from the computational results that the proposed method has a high accuracy and still remains stable when time step is 10 times of the Courant stability condition. Computational cost can be saved by more than 70% compared with the conventional RPIM method.

1. INTRODUCTION

Meshless techniques have existed for almost 30 years. Unlike conventional simulation algorithms [1–7], which relies on a grid or a mesh, meshless techniques, in contrast, use scattered nodes to represent the spatial solving area as shown in Figure 1. These nodes can be placed randomly in the solution region, and no strict limitation between adjacent nodes is required, thus make the meshless methods more flexible for solving EM problems, especially for those which have curved and slopped boundaries.

Among all the various meshless methods, the local radial point interpolation method (RPIM) [8] is a robust and numerical one which uses the radial basis functions (RBFs) to construct the field

Received 6 May 2013, Accepted 6 July 2013, Scheduled 10 July 2013

* Corresponding author: Feijiao Liu (helllady@163.com).

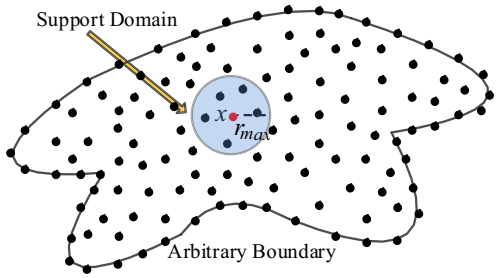

Figure 1. Spatial discretization of solution region and support domain of a point of interest.

function. It has the advantages of conformal modeling of arbitrary boundaries and capabilities of the multi-scale solutions. The RPIM meshless method was firstly applied to solving time-domain EM problems by Kaufmann et al. [9]. Kaufmann et al. also made detailed description of the conformal and multi-scale capabilities of the method [10, 11]. Lai et al. introduced the numerical stability and dispersion of RPIM in detail [12], Tanaka and Kunisada applied RPIM meshless method cooperated with Newmark's β method to solve transient electromagnetic field [13]. Yu and Chen extended the RPIM method to 3-D conditions and discussed the numeral stability conditions [14].

In order to avoid the Courant stability condition, Yu and Chen proposed an unconditionally stable time-domain meshless method which applied the alternating-direction-implicit (ADI) scheme in the 3-D RPIM meshless method called ADI-RPIM [15]. They also proposed a systematic approach to accurate imposition of material interface conditions for the RPIM [16] and applied the conventional perfectly matched layer (CPML) absorbing boundary conditions to the RPIM [17].

Another unconditionally stable meshless method was developed by Chen et al. recently [18]. In their method, weighted Laguerre polynomials were applied to corporate with RPIM. The weighted Laguerre polynomials were applied earlier in the finite-difference time-domain (FDTD) method to develop an unconditionally stable scheme called Laguerre-FDTD [19, 20]. However, both the Laguerre-FDTD and Chen's method are limited to 2-D conditions.

The purpose of this paper is to develop a 3-D unconditionally stable RPIM meshless method with the weighted Laguerre polynomials. The derivation of Laguerre-RPIM meshless method will be given in Section 2. In Section 3, two numerical examples will be presented to verify the accuracy and efficiency of the proposed method. The

conclusions will be made in the end.

2. THE PROPOSED 3-D LAGUERRE-RPIM METHOD

2.1. The Conventional RPIM Method

As a robust meshless method, the RPIM method has the advantages of arbitrary nodal distribution and conformal modeling of giving problems. The field function $u(\mathbf{r})$ is approximated by:

$$u(\mathbf{r}) = \sum_{n=1}^{N} r_n(\mathbf{r}) a_n + \sum_{m=1}^{M} p_m(\mathbf{r}) b_m \tag{1}$$

where $\mathbf{r} = (x, y, z)$ is the point of interest, $r_n(\mathbf{r})$ the radial basis function [9], $p_m(\mathbf{r})$ the monomial basis function, a_n and b_m the corresponding coefficients, N the number of nodes within the support domain (Figure 1) of the interested point used for the interpolation, and M the order of the monomial basis.

After several times of transformation [9], the field quantity $u(\mathbf{r})$ can be expressed by the nodal field value u_n within the support domain as

$$u(\mathbf{r}) = \sum_{n=1}^{N} \phi_n(\mathbf{r}) u_n \tag{2}$$

where $\phi_n(\mathbf{r})$ is the shape function of the nth node in the support domain [9].

Then the spatial derivation of the field function can be obtained

$$\frac{\partial u(\mathbf{r})}{\partial \kappa} = \sum_{n=1}^{N} \frac{\partial \phi_n(\mathbf{r})}{\partial \kappa} u_n \tag{3}$$

where $\kappa = x, y, z$.

For TM-to-z waves, the time-domain Maxwell's equations can be discretized by applying (2) and (3). With the definition of E and H nodes, the field variables and corresponding spatial derivatives can be approximated while the central difference is still used to approximate the time derivatives; the resulting leapfrog meshless RPIM formulations are [9]:

$$H_x^{n+1/2}(\mathbf{r}) = H_x^{n-1/2}(\mathbf{r}) - \frac{\Delta t}{\mu(\mathbf{r})} \sum_{j=1}^{N_j} E_{z,j}^n \frac{\partial \phi_j(\mathbf{r})}{\partial y} \tag{4}$$

$$H_y^{n+1/2}(\mathbf{r}) = H_y^{n-1/2}(\mathbf{r}) + \frac{\Delta t}{\mu(\mathbf{r})} \sum_{j=1}^{N_j} E_{z,j}^n \frac{\partial \phi_j(\mathbf{r})}{\partial x} \tag{5}$$

$$E_z^{n+1}(\mathbf{r}) = E_z^{n-1}(\mathbf{r}) + \frac{\Delta t}{\varepsilon(\mathbf{r})}\left(\sum_{i=1}^{N_i} H_{y,i}^{n+1/2}\frac{\partial \phi_i(\mathbf{r})}{\partial x} - \sum_{i=1}^{N_i} H_{x,i}^{n+1/2}\frac{\partial \phi_i(\mathbf{r})}{\partial y}\right) \quad (6)$$

where N_j is the number of H nodes in the support domain of interested E node and N_i is the number of H nodes in the support domain of interested E node.

2.2. The Proposed Unconditionally Stable Laguerre-RPIM Meshless Method

The Laguerre polynomial of order p is defined as:

$$L_p(t) = \frac{e^t}{p!}\frac{d^p}{dt^p}\left(t^p e^{-t}\right) \quad \text{for} \quad p \geq 0;\ t \geq 0. \quad (7)$$

The Laguerre polynomials are orthogonal with respect to the weighting function e^{-t}, expressed as

$$\int_0^\infty e^{-t} L_p(t) L_q(t) dt = \delta_{pq} \quad (8)$$

Thus, an orthogonal set of basis function $\{f_0, f_1, f_2, \ldots\}$ can be constructed as [18]:

$$f_p(t) = e^{-t/2} L_p(t) \quad (9)$$

As $t \to \infty$, the weighted Laguerre basis functions converge to zero. Then any field component concerned can be expressed as

$$U(\mathbf{r}, t) = \sum_{p=0}^{\infty} U^p(\mathbf{r}) f_p(t) \quad (10)$$

In this paper, for the sake of simplicity and perspicuity, we use E_z component as representative to obtain the final required equation. The formulation of Maxwell's equation can be expressed as:

$$\frac{\partial E_z(\mathbf{r}, t)}{\partial t} = \frac{1}{\varepsilon}\left[\frac{\partial H_y(\mathbf{r}, t)}{\partial x} - \frac{\partial H_x(\mathbf{r}, t)}{\partial y} - J_z\right] \quad (11)$$

The time-domain field quantity can be expanded within the weighted Laguerre polynomials as:

$$E_z(\mathbf{r}, t) = \sum_{p=0}^{\infty} E_z^p(\mathbf{r}) f_p(st) \quad (12)$$

where $E_z^p(\mathbf{r})$ is the relate expansion coefficients and the basis function $f_p(st)$ the weighted Laguerre polynomials of order p. $s > 0$ is a time scale factor using for adjusting the time variable t to an appropriate

amplitude for calculation [21]. Since the real time scale is quite small, in order to use the above basis functions properly, one should transform the real time scale using an appropriate scale factor.

For $E_z(\mathbf{r}, t)$ expressed as (12) which satisfies

$$E_z(\mathbf{r}, 0) = \sum_{p=0}^{\infty} E_z^p(\mathbf{r}) f_p(0) = \sum_{p=0}^{\infty} E_z^p(\mathbf{r}) = 0 \tag{13}$$

its first-order temporal derivative with respect to time t can be expressed as [19, 22]:

$$\frac{\partial E_z(\mathbf{r}, t)}{\partial t} = s \sum_{p=0}^{\infty} \left(0.5 E_z^p(\mathbf{r}) + \sum_{k=0, p>0}^{p-1} E_z^k(\mathbf{r}) \right) f_p(st) \tag{14}$$

By inserting (12), (14) into (11), the equations can be rewritten as:

$$\begin{aligned} & s \sum_{p=0}^{\infty} \left(0.5 E_z^p(\mathbf{r}) + \sum_{k=0, p>0}^{p-1} E_z^k(\mathbf{r}) \right) f_p(st) \\ = & \frac{1}{\varepsilon(\mathbf{r})} \sum_{p=0}^{\infty} \left[\frac{\partial}{\partial x} H_y^p(\mathbf{r}) - \frac{\partial}{\partial y} H_x^p(\mathbf{r}) \right] f_p(st) - \frac{1}{\varepsilon(\mathbf{r})} J_z(\mathbf{r}) \end{aligned} \tag{15}$$

Multiply $f_p(st)$ in both sides and then integrate expression of both sides of the equal sign in the time domain. According to (8), we can have:

$$\begin{aligned} E_z^p(\mathbf{r}) = & \frac{2}{\varepsilon(\mathbf{r}) s} \sum_{i=1}^{N_i} \left[\frac{\partial \phi_i(\mathbf{r})}{\partial x} H_{y,i}^p - \frac{\partial \phi_i(\mathbf{r})}{\partial y} H_{x,i}^p \right] \\ & -2 \sum_{k=0, p>0}^{p-1} E_z^k(\mathbf{r}) - \frac{2}{\varepsilon(\mathbf{r}) s} J_z^p(\mathbf{r}) \end{aligned} \tag{16}$$

where

$$J_z^p(\mathbf{r}) = \int_0^{T_f} J_z(\mathbf{r}, t) f_p(st)\, s dt \tag{17}$$

Similarly, we can get the remainning 5 other equations expressed as:

$$H_x^p(\mathbf{r}) = \frac{2}{s\mu(\mathbf{r})} \sum_{j=1}^{N_j} \left[E_{y,j}^p \frac{\partial \phi_j(\mathbf{r})}{\partial z} - E_{z,j}^p \frac{\partial \phi_j(\mathbf{r})}{\partial y} \right] - 2 \sum_{k=0, p>0}^{p-1} H_x^k(\mathbf{r}) \tag{18}$$

$$H_y^p(\mathbf{r}) = \frac{2}{s\mu(\mathbf{r})} \sum_{j=1}^{N_j} \left[E_{z,j}^p \frac{\partial \phi_j(\mathbf{r})}{\partial x} - E_{x,j}^p \frac{\partial \phi_j(\mathbf{r})}{\partial z} \right] - 2 \sum_{k=0,p>0}^{p-1} H_y^k(\mathbf{r}) \quad (19)$$

$$H_z^p(\mathbf{r}) = \frac{2}{s\mu(\mathbf{r})} \sum_{j=1}^{N_j} \left[E_{x,j}^p \frac{\partial \phi_j(\mathbf{r})}{\partial y} - E_{y,j}^p \frac{\partial \phi_j(\mathbf{r})}{\partial x} \right] - 2 \sum_{k=0,p>0}^{p-1} H_z^k(\mathbf{r}) \quad (20)$$

$$E_x^p(\mathbf{r}) = \frac{2}{s\varepsilon(\mathbf{r})} \sum_{i=1}^{N_i} \left[H_{z,i}^p \frac{\partial \phi_i(\mathbf{r})}{\partial y} - H_{y,i}^p \frac{\partial \phi_i(\mathbf{r})}{\partial z} \right] - 2 \sum_{k=0,p>0}^{p-1} E_x^k(\mathbf{r}) - \frac{2}{s\varepsilon(\mathbf{r})} J_x^p(\mathbf{r}) \quad (21)$$

$$E_y^p(\mathbf{r}) = \frac{2}{s\varepsilon(\mathbf{r})} \sum_{i=1}^{N_i} \left[H_{x,i}^p \frac{\partial \phi_i(\mathbf{r})}{\partial z} - H_{z,i}^p \frac{\partial \phi_i(\mathbf{r})}{\partial x} \right] - 2 \sum_{k=0,p>0}^{p-1} E_y^k(\mathbf{r}) - \frac{2}{s\varepsilon(\mathbf{r})} J_y^p(\mathbf{r}) \quad (22)$$

By substituting (18) and (19) into (16), we can have the final expression of $E_z^p(\mathbf{r})$

$$E_z^p(\mathbf{r}) - \alpha(\mathbf{r}) \sum_{i=1}^{N_i} \sum_{j=1}^{N_j} \left[\frac{\partial \phi_i(\mathbf{r})}{\partial x} \frac{\partial \phi_j(\mathbf{r}_i)}{\partial x} + \frac{\partial \phi_i(\mathbf{r})}{\partial y} \frac{\partial \phi_j(\mathbf{r}_i)}{\partial y} \right] E_{z,j}^p$$

$$+\alpha(\mathbf{r}) \sum_{i=1}^{N_i} \sum_{j=1}^{N_j} \frac{\partial \phi_i(\mathbf{r})}{\partial x} \frac{\partial \phi_j(\mathbf{r}_i)}{\partial z} E_{x,j}^p + \alpha(\mathbf{r}) \sum_{i=1}^{N_i} \sum_{j=1}^{N_j} \frac{\partial \phi_i(\mathbf{r})}{\partial y} \frac{\partial \phi_j(\mathbf{r}_i)}{\partial z} E_{y,j}^p$$

$$= \beta_z^{p-1} - \beta(\mathbf{r}) J_z^p(\mathbf{r}) \quad (23)$$

where $\alpha(\mathbf{r}) = \frac{4}{s^2 \mu(\mathbf{r}) \varepsilon(\mathbf{r})}$, $\beta(\mathbf{r}) = \frac{2}{s\varepsilon(\mathbf{r})}$ and

$$\beta_z^{p-1} = 2 \sum_{k=0,p>0}^{p-1} E_z^k(\mathbf{r}) + 2\beta(\mathbf{r}) \sum_{i=1}^{N_i} \sum_{k=0,p>0}^{p-1} \frac{\partial \phi_i(\mathbf{r})}{\partial y} H_x^k(\mathbf{r}_i) - 2\beta(\mathbf{r}) \sum_{i=1}^{N_i} \sum_{k=0,p>0}^{p-1} \frac{\partial \phi_i(\mathbf{r})}{\partial x} H_y^k(\mathbf{r}_i) \quad (24)$$

$E_x^p(\mathbf{r})$ and $E_y^p(\mathbf{r})$ can be derived in a similar manner. They are listed as follows

$$E_x^p(\mathbf{r}) - \alpha(\mathbf{r}) \sum_{i=1}^{N_i} \sum_{j=1}^{N_j} \left[\frac{\partial \phi_i(\mathbf{r})}{\partial y} \frac{\partial \phi_j(\mathbf{r}_i)}{\partial y} + \frac{\partial \phi_i(\mathbf{r})}{\partial z} \frac{\partial \phi_j(\mathbf{r}_i)}{\partial z} \right] E_{x,j}^p$$

$$+\alpha(\mathbf{r})\sum_{i=1}^{N_i}\sum_{j=1}^{N_j}\frac{\partial\phi_i(\mathbf{r})}{\partial y}\frac{\partial\phi_j(\mathbf{r}_i)}{\partial x}E_{y,j}^p+\alpha(\mathbf{r})\sum_{i=1}^{N_i}\sum_{j=1}^{N_j}\frac{\partial\phi_i(\mathbf{r})}{\partial z}\frac{\partial\phi_j(\mathbf{r}_i)}{\partial x}E_{z,j}^p$$
$$=\beta_x^{p-1}-\beta(\mathbf{r})J_x^p(\mathbf{r}) \tag{25}$$

$$E_y^p(\mathbf{r})-\alpha(\mathbf{r})\sum_{i=1}^{N_i}\sum_{j=1}^{N_j}\left[\frac{\partial\phi_i(\mathbf{r})}{\partial x}\frac{\partial\phi_j(\mathbf{r}_i)}{\partial x}+\frac{\partial\phi_i(\mathbf{r})}{\partial z}\frac{\partial\phi_j(\mathbf{r}_i)}{\partial z}\right]E_{y,j}^p$$
$$+\alpha(\mathbf{r})\sum_{i=1}^{N_i}\sum_{j=1}^{N_j}\frac{\partial\phi_i(\mathbf{r})}{\partial x}\frac{\partial\phi_j(\mathbf{r}_i)}{\partial y}E_{x,j}^p+\alpha(\mathbf{r})\sum_{i=1}^{N_i}\sum_{j=1}^{N_j}\frac{\partial\phi_i(\mathbf{r})}{\partial z}\frac{\partial\phi_j(\mathbf{r}_i)}{\partial y}E_{z,j}^p$$
$$=\beta_y^{p-1}-\beta(\mathbf{r})J_y^p(\mathbf{r}) \tag{26}$$

where

$$\begin{aligned}\beta_x^{p-1} &= -2\sum_{k=0,p>0}^{p-1}E_x^k(\mathbf{r})+2\beta(\mathbf{r})\sum_{i=1}^{N_i}\sum_{k=0,p>0}^{p-1}\frac{\partial\phi_i(\mathbf{r})}{\partial z}H_y^k(\mathbf{r}_i)\\ &\quad -2\beta(\mathbf{r})\sum_{i=1}^{N_i}\sum_{k=0,p>0}^{p-1}\frac{\partial\phi_i(\mathbf{r})}{\partial y}H_z^k(\mathbf{r}_i)\end{aligned} \tag{27}$$

$$\begin{aligned}\beta_y^{p-1} &= -2\sum_{k=0,p>0}^{p-1}E_y^k(\mathbf{r})+2\beta(\mathbf{r})\sum_{i=1}^{N_i}\sum_{k=0,p>0}^{p-1}\frac{\partial\phi_i(\mathbf{r})}{\partial x}H_z^k(\mathbf{r}_i)\\ &\quad -2\beta(\mathbf{r})\sum_{i=1}^{N_i}\sum_{k=0,p>0}^{p-1}\frac{\partial\phi_i(\mathbf{r})}{\partial z}H_x^k(\mathbf{r}_i)\end{aligned} \tag{28}$$

The above three equations are applied at each node position and then a final matrix can be obtained which has the formulation as:

$$[A]\{E^p\}=\{J^p\}+\left\{\beta^{p-1}\right\},\quad p=0,1,2,\ldots \tag{29}$$

where

$$\begin{aligned}E^p&=\left\{E_{x,1}^p,E_{y,1}^p,E_{z,1}^p,\ldots,E_{x,j}^p,E_{y,j}^p,E_{z,j}^p,\ldots\right\}^T\\ J^p&=\left\{J_{x,1}^p,J_{y,1}^p,J_{z,1}^p,\ldots,J_{x,j}^p,J_{y,j}^p,J_{z,j}^p,\ldots\right\}^T\\ \beta^{p-1}&=\left\{\beta_{x,1}^{p-1},\beta_{y,1}^{p-1},\beta_{z,1}^{p-1},\ldots,\beta_{x,j}^{p-1},\beta_{y,j}^{p-1},\beta_{z,j}^{p-1},\ldots\right\}^T\end{aligned} \tag{30}$$

The matrix $[A]$ is decided by μ, ε and ϕ, and it is independent from the expanded function order p. Equation (29) can be computed in a recursive manner. All the expansion coefficients can be solved by

marching in order p. Then the field component can be acquired by applying (12).

It can be observed from (12) that $p \to \infty$ which cannot be done in the actual situation. Here we choose N_L as the maximum order of the expanded functions. It is determined by [21]

$$N_L = 2BT_f + 1 \tag{31}$$

where T_f is the temporal duration of time and $2B$ the bandwidth of the excitation source.

According upper equations, we can find out that the dimension of the final matrix is $3N \times 3N$. As previously mentioned, the Laguerre-RPIM uses the local support domain to construct shape function which makes the final matrix banded and sparse. Through the already existed large sparse matrix solver, the whole computing efficiency can be greatly improved. Here the unsymmetrical multifrontal sparse LU factorization package (UMFPACK) is used to solve (29).

3. NUMERAL EXAMPLES

Two examples were chosen here to verify the proposed Laguerre-RPIM method, one being a rectangular cavity and the other being a perfect conducting quarter-ring resonator. In the two examples, a modulated Gaussian pulse is chosen as an exciting current source given by

$$J_z(t) = \exp\left[-\left(\frac{t-t_0}{\tau}\right)^2\right] \sin\left[2\pi f_c (t-t_0)\right] \tag{32}$$

where $f_c = 3\,\text{GHz}$, $\tau = \frac{1}{f_c}$, $t_0 = 4\tau$.

Here, the Gaussian function is chosen as the radial basis function. It is expressed as

$$r_n(\mathbf{r}) = e^{-c(r/r_{\max})^2} \tag{33}$$

where $r = \sqrt{(x-x_n)^2 + (y-y_n)^2 + (z-z_n)^2}$, (x_n, y_n, z_n) is the coordinates of the nth node included in the support domain of $\mathbf{r}$, c the shape parameter, and $r_{\max}$ the radius of the support domain of the interested point (Figure 1).

The size of the support domain $r_{\max}$ is chosen to be twice of the largest distance between two adjacent points. Scale factor and number of temporal basis functions is chosen to be $s = 6 \times 10^{10}$, $N_L = 250$.

The electric and magnetic field nodes are staggered in space as shown in Figure 2. Each E node is surrounded by six magnetic field nodes, and each H node is surrounded by two electric fields. Thus the nodes in whole solution region are linked together which makes the final matrix nonsingular and sparse.

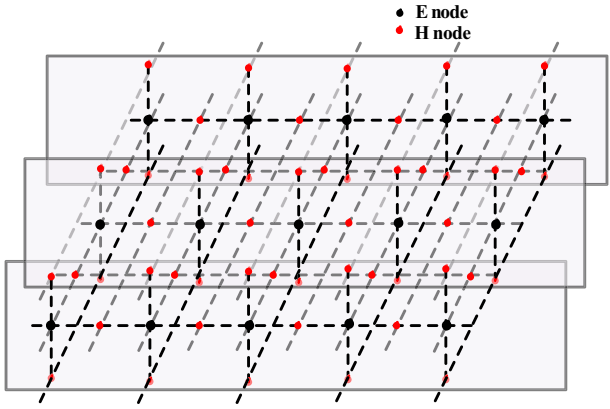

Figure 2. Nodal distribution stratergy for time-domain meshless method.

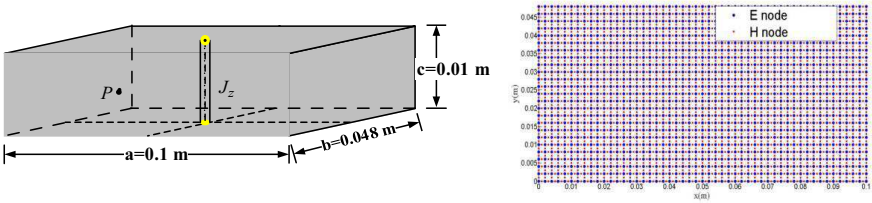

Figure 3. Geometry and node distribution of the 3-D rectangular cavity. (a) Geometry of the 3-D rectangular cavity. (b) Node distribution in the x-y plane.

3.1. 3-D Rectangular Cavity

The first example used here is a 3-D rectangular cavity which is applied to verify the accuracy of the proposed method. The geometry of the cavity is depicted in Figure 3. The resonant frequency of the cavity can be obtained through theoretical calculations:

$$f_{mnl} = \frac{c}{2\pi\sqrt{\mu_r \varepsilon_r}} \sqrt{\left(\frac{m\pi}{a}\right)^2 + \left(\frac{n\pi}{b}\right)^2 \left(\frac{l\pi}{d}\right)^2} \tag{34}$$

where m, n, l represents the number of wave pattern changes in each direction of x, y, z, and a, b, d represents the size of this rectangular cavity. The cavity was discretized by regularly distributed E nodes and H nodes with a common nodal distance of 0.002 m as shown in Figure 3. The position of the exciting point and observing point can also be seen

in Figure 3. The Analytical Solution can be obtained from (42). The resonant frequency of TE_{110} or TM_{110} mode is 3.4664 GHz.

The conventional RPIM method was also chosen here for comparison. The time-domain electric field recorded at the observation point and its Fourier transform is plotted in Figure 4. As can be seen from the plots, the agreement between the results obtained with the conventional RPIM method and those obtained with the proposed Laguerre-RPIM method is very good. The simulated resonant frequency has very small difference compared with the accurate value.

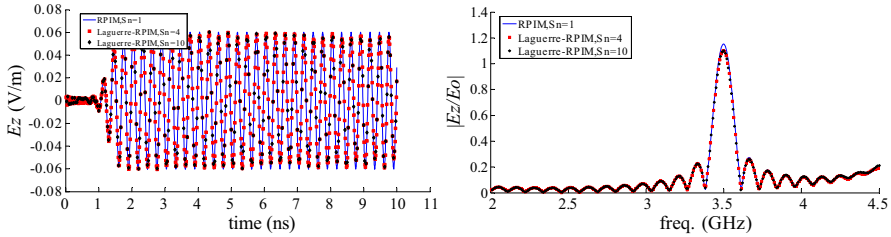

Figure 4. The electric field recorded at observation point of the 3-D rectangular cavity: (a) The electric field recorded at observation point. (b) Normalized frequency-domain E_Z field at the observation point.

Table 1. Memory required and CPU time cost in computing the rectangular cavity.

	Conventional RPIM method	Proposed Laguerre-RPIM method		Analytical Solution
Stability Number (Sn)	1	4	10	
Memory Requirement (Mb)	13.34	19.35	19.51	
Computational Time (s)	42.79	13.46	12.36	
Resonant Frequency (GHz)	3.49875	3.4987	3.4987	3.4664

*All simulations were performed on a Inter® Core™ 2 Duo PC with a CPU of 2.2 GHz and a RAM of 2GB

Table 1 gives the comparison of simulated and theoretical resonant frequency values. S_n represent multiples of the Courant stability condition which is the maximum time step used in conventional RPIM method. It shows that the difference of the resonant frequency is small enough to be negligible. Also the memory and CPU time used are involved. The CPU time cost of the proposed method is only 30% of the conventional RPIM meshless method.

3.2. A 3-D Perfect Conducting Quarter-ring Resonator

The 3-D perfect conducting quarter-ring resonator is chosen to test the unconditional stability and verify the computational effectiveness of the proposed method.

The geometry of the resonator is depicted in Figure 5. The position of the exciting point and observing point can also be seen in Figure 5. The solution domain is discretized by scattered nodes in a conformal way. It has a radial pattern: the nodes are denser close to the inner conducting wall and are coarser when approaching the outer conducting wall. The smallest nodal distance between two neighboring nodes is 0.001 m and the largest distance between the nodes is 0.0047 m. The ratio of the largest distance between the nodes to the smallest is 4.7.

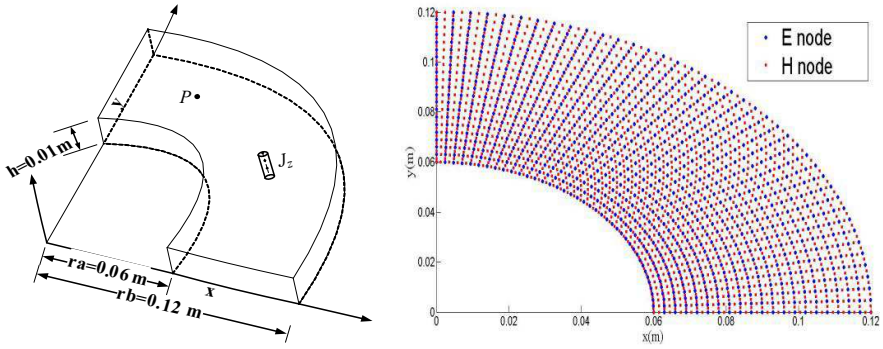

(a) (b)

Figure 5. Geometry and node distribution of the 3-D perfect conducting quarter-ring resonator. (a) Geometry of the 3-D Perfect Conducting Quarter-ring Resonator. (b) Node distribution in the x-y plane.

As described above, the conventional RPIM method is used here for comparison. The simulated electric fields at the observed point and its Fourier transform of the time-domain values are plotted in Figure 6.

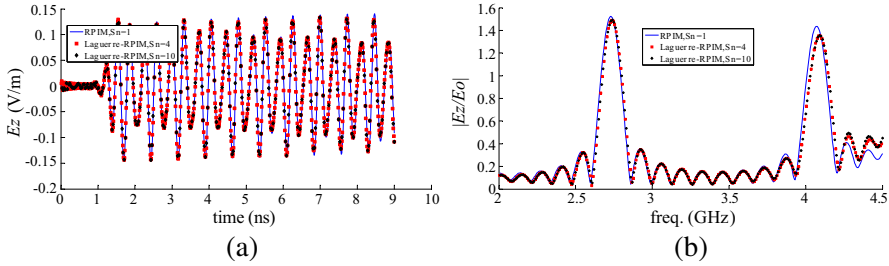

Figure 6. The electric field recorded at observation point of the 3-D perfect conducting quarter-ring resonator. (a) The electric field recorded at observation point. (b) Normalized frequency-domain E_Z field at the observation point.

As can be observed from the figures, the agreement between the results of these two methods is quit fine. Also, the proposed unconditionally stable meshless method presents stable solutions even when the time step is ten times the Courant stability condition. The numerical tests with even larger time steps were made and the result shows still stable.

Table 2 lists the computational cost and memory requirement of these two methods. When simulation time is chosen to be ten times the Courant stability condition, the proposed unconditionally stable meshless method can reduce the simulation time by up to 70%. Since the proposed method contains the storage and solving of large matrix, extra memory is required to store the non-zero elements of

Table 2. Memory required and CPU time cost in computing the quarter-ring resonator.

	Conventional RPIM method	Proposed Laguerre-RPIM method	
Stability Number (Sn)	1	4	10
Memory Requirement (Mb)	9.14	15.05	15.02
Computational Time (s)	32.27	21.42	20.21

*All simulations were performed on a Inter® Core™ 2 Duo PC with a CPU of 2.2 GHz and a RAM of 2GB

the matrix equations. However, the large saving in the computational time becomes insignificant comparing with the merits of larger time steps and less number of iterations especially due to the advance of computer technology.

4. CONCLUSION

In this paper, a new 3-D time-domain meshless method is presented. The RBFs are applied to construct the shape function, and the weighted Laguerre polynomials are used to express field component and its derivative. With the decaying nature of Laguerre polynomials the final scheme is unconditionally stable. Two examples are chosen to verify the effectiveness and efficiency of the proposed method. Numeral examples suggest a high accuracy and time saving can be more than 70% compared with the conventional RPIM method.

The electromagnetic computation of the open structures using the proposed method will be studied in the future.

ACKNOWLEDGMENT

This work was supported by the National Natural Science Foundation of China (No. 60831001) and the South Wisdom Valley Innovative Research Team Program. The authors wish to give special thanks to Xiaojie Chen for her pioneering work in this field and Xiaotong Mu for his sincere help in EMC Technique Institute of Beihang University.

REFERENCES

1. Yee, K. S., "Numerical solution of initial boundary value problems involving Max-well's equations in isotropic media," *IEEE Trans. on Antennas on Propag.*, Vol. 14, No. 3, 302–307, 1966.
2. Vaccari, A., A. Cala' Lesina, L. Cristoforetti, and R. Pontalti, "Parallel implementation of a 3D subgridding FDTD algorithm for large simulations," *Progress In Electromagnetics Research*, Vol. 120, 263–292, 2011.
3. Klopf, E. M., S. B. Manic, M. M. Ilic, and B. M. Notaroš, "Efficient time-domain analysis of waveguide discontinuities using higher order FEM in frequency domain," *Progress In Electromagnetics Research*, Vol. 120, 215–234, 2011.
4. Zhao, L. and K.-L. Wu, "A hybrid NFM/MoM full-wave analysis of layered prolate head model exposed to handset

antenna," *Progress In Electromagnetics Research*, Vol. 123, 205–225, 2012.

5. Wang, J.-B., B.-H. Zhou, L.-H. Shi, C. Gao, and B. Chen, "A novel 3-D weakly conditionally stable FDTD algorithm," *Progress In Electromagnetics Research*, Vol. 130, 525–540, 2012.
6. Kong, Y.-D., Q.-X. Chu, and R.-L. Li, "High-order unconditionally-stable four-step ADI-FDTD methods and numerical analysis," *Progress In Electromagnetics Research*, Vol. 135, 713–734, 2013.
7. Fotyga, G., K. Nyka, and M. Mrozowski, "Efficient model order reduction for FEM analysis of waveguide structures and resonators," *Progress In Electromagnetics Research*, Vol. 127, 277–295, 2012.
8. Wang, J. G. and G. R. Liu, "A point interpolation meshless method based on radial basis i functions," *Int. J. Numer. Methods Eng.*, Vol. 54, 1623–1648, 2001.
9. Kaufmann, T., C. Fumeaux, and R. Vahldieck, "The meshless radial point interpolation method for time-domain electromagnetics," *Digests of IEEE MTT-S Int. Microw. Symp.*, 61–64, Atlanta, GA, Jun. 15–20, 2008.
10. Kaufmann, T., C. Fumeaux, and C. Engstrom, "A comparison of three meshless algorithms: Radial point interpolation, non-symmetric and symmetric Kansa method," *Digests of IEEE MTT-S Int. Microw. Symp.*, 1–4, Atlanta, GA, Jun. 5–10, 2011.
11. Fumeaux, C., T. Kaufmann, D. Baumann, and M. Klemm, "Conformal and multi-scale time-domain methods: From tetrahedral mesh to meshless discretisation," *2012 Asia-Pacific Symposium on Electromagnetic Compatibility (APEMC)*, 161–164, May 21–24, 2012.
12. Lai, S. J., B. Z. Wang, and Y. Duan, "Meshless radial basis function method for transi-ent electromagnetic computations," *IEEE Trans. on Magnetics*, Vol. 44, No. 10, 2288–2295, 2008.
13. Tanaka, Y. and E. Kunisada, "Study on meshless method using RPIM for transient electromagnetic field," *IEEE Trans. on Magnetics*, Vol. 47, No. 5, 1178–1181, May 2011.
14. Yu, Y. and Z. Chen, "A 3-D radial point interpolation method for meshless time-domain modeling," *IEEE Trans. on Microwave Theory and Tech.*, Vol. 57, No. 8, 2015–2020, Aug. 2009.
15. Yu, Y. and Z. Chen, "Towards the development of unconditionally stable time-domain meshless numerical methods," *IEEE Trans. on Microwave Theory and Tech.*, Vol. 58, No. 3, 578–586, Mar. 2010.

16. Yu, Y. and Z. Chen, "Implementation of material interface conditionsin the radial point interpolation meshless method," *IEEE Trans. on Antennas and Propag.*, Vol. 59, No. 8, 2916–2923, 2011.
17. Yu, Y. and Z. Chen, "Meshless RPIM modeling of open-structures using PMLs," *Digest of the 2010 IEEE International Microwave Symposium*, 1, Anaheim, May 23–28, 2010.
18. Chen, X., Z. Chen, Y. Yu, and D. Su, "An unconditionally stable radial point interpolation meshless method with Laguerre polynomials," *IEEE Trans. on Antennas and Propag.*, Vol. 59, No. 10, 3756–3763, Oct. 2011.
19. Chung, Y. S., T. K. Sarkar, B. H. Jung, and M. Salazar-Palma, "An unconditionally stable scheme for the finite-difference time-domain method," *IEEE Trans. on Microwave Theory and Tech.*, Vol. 51, No. 3, 697–704, Mar. 2003.
20. Srinivasan, K., M. Swaminathan, and E. Engin, "Overcoming limitations of Laguerre-FDTD for fast time-domain EM simulation," *IEEE Int. Microwave Symp. Digest*, 891–894, 2007.
21. Lacik, J., "Laguerre polynomials' scheme of transient analysis: Scale factor and number of temporal basis functions," *Radioengineering*, Vol. 18, No. 1, 23–28, 2009.
22. Ha, M. and M. Swaminathan, "A Laguerre-FDTD formulation for frequency-dependent dispersive materials," *IEEE Microw. Wireless Compon. Lett.*, Vol. 21, No. 5, 225–227, Mar. 2011.